Accuracy of the moment-tensor inversion of far-field P waves

Yue Kong[1] , Min Li[1] , Weimin Chen[2] and Boqi Kang[3]

1 School of Aeronautic Science and Engineering, Beihang University, Beijing 100083, R.P China.

2 Institute of Mechanics, Chinese Academy of Sciences, Beijing 100190, R.P. China. E-mail: wmchen@imech.ac.cn

3 Key Laboratory of Space Utilization, Technology and Engineering Center for space Utilization, Chinese Academy of Sciences, Beijing 100094, R.P China.

SUMMARY: The far-field assumption is widely used and suitable for the moment-tensor inversion, in which the source-receiver distance is quite long. However, the description of far field is uncertain and an explicit far-field range is missing. In this study, the explicit far-field range is determined and the errors of moment-tensor solutions produced by the far-field approximation are analyzed. The distance, for which the far-field assumption is satisfied and the effect of the near-field term can be ignored, is directionally dependent. For the shear dislocation, in the directions near the nodal lines of the far-field P waves, the far-field distance is heavily dependent on the displacement component used to invert moment tensors. The radial component of displacement, which is parallel to the wave propagation direction, is recommended for the inversion and the corresponding far-field distance is quite short. In the directions far from the nodal lines, the selection of displacement components has little influence on the far-field distance. The maximum far-field distance appears in the directions of the pressure and tensile axes of the source and the value is about 30 wavelengths of

radiated waves. Using more receivers (>6) in the moment-tensor inversion can shorten the far-field distance. The effect of the near-field term on the moment-tensor inversion for tensile dislocations and isotropic sources (explosion or implosion) can be ignored. The conclusions obtained in this study are helpful for determining the positions of receivers and evaluating the accuracy of moment-tensor solutions, with far-field assumption being applied in the inversion.

Keywords: Earthquake source observations; Inverse theory; Wave propagation; Body waves

1 INTRODUCTION

Interpreting the source mechanisms of seismic events is important for understanding the evolution of stress field (Der Baan *et al.* 2016; Eaton *et al.* 2014) and provides an insight into source properties. A common method of calculating source mechanisms is the moment-tensor inversion, which can provide the knowledge of fracture type and propagation (Silený 2009; Vavryčuk 2001). The moment-tensor inversion utilizes the radiation pattern of seismic waves to obtain a 3×3 symmetric matrix, in which each component represents a force couple (Aki & Richards 1980). Compared with surface waves (Aki & Patton 1978; Kanamori & Given 1981; Kanamori & Given 1982), the usage of body waves (Ohtsu 1988; Ohtsu & Ono 1988) in the moment-tensor inversion can simplify the inversion and is common in the engineering practice. Moment tensors can be calculated using the amplitude of seismic waves (Fojtíková *et al.* 2010; Vavryčuk *et al.* 2008), amplitude ratios (Hardebeck & Shearer 2003; Jechumtalova & Silený 2005) or full wave forms (Dziewonski *et al.* 1981; Silený *et al.* 1992; Sipkin 1986). For physically interpreting source mechanisms, the decompositions and source-type plots of moment tensors were provided (Hudson *et al.* 1989; Tape & Tape 2012;

Vavryčuk 2001; Vavryčuk 2015).

In the moment-tensor inversion, the Green's function is extremely important and has been provided by Aki & Richards (1980) for simple types of media. Actually, the function used in the moment tensor inversion is the spatial derivatives of the Green's function, which is called the Green's function of second kind. According to distance, seismic waves consist of two parts, the near-field and far-field terms. For simplifying the moment-tensor inversion, the far-field term is supposed to be dominated and the effect of the near-field term on moment-tensor solutions is ignored. The far-field assumption has been widely applied in earthquake monitoring (Cesca *et al.* 2006; Lizurek 2017; Trifu 2000) and rock damage experiments (Graham *et al.* 2010; Stierle *et al.* 2016; Xu *et al.* 2017; Yu *et al.* 2005), in which the source-receiver distances are always quite long. In some specific engineering practices, the source-receiver distances are obviously very short and the far-field assumption is not suitable for the moment-tensor inversion, such as the volcano seismology (Legrand *et al.* 2000; Lokmer & Bean 2010; Van Driel *et al.* 2015).

Although many investigations (Nissen-Meyer *et al.* 2007; Toyokuni & Takenaka 2006; Van Driel & Nissenmeyer 2014) analyzed the waveforms caused by seismic sources, the far-field term is never studied separately and the boundary of far field is quite uncertain. Aki & Richards (1980) provided a simple definition of far field that distance of the receiver should be larger than a few wavelengths away from the source. But no more details about the number of wavelengths are specified. For example, Liu *et al.* (2014) assumed the number of wavelengths as 4. By contrast, Vidale *et al.* (1995) pointed out that the near-field term can be observable at great distance from a very large deep earthquake in some cases. It can be

concluded that the boundary between the near and far field is uncertain, and one must assess the relative magnitude of each term (Aki & Richards 1980). For some earthquakes with shallow depth, it is quite uncertain whether the source-receiver distance is long enough and the error caused by the far-field assumption can be ignored. In addition, the traditional description of far-field range is based on the relative magnitude of the two terms (Aki & Richards 1980), which can not indicate the errors of moment-tensor solutions directly. Consequently, it is significant to clarify the far-field range and analyze the errors of moment-tensor solutions caused by the far-field assumption. In the study, the moment-tensor inversion is carried out based on synthetic data and the explicit far-field range is determined by the errors of moment-tensor solutions. The sensitivity of far-field range to several factors, which are the wave velocity, frequency, positions of receivers and source mechanism, is analyzed.

2 THEORETICAL ANALYSIS

2.1 Formulations

The moment tensor of seismic sources in isotropic media is expressed as follows:

$$m_{pq} = \lambda l_k n_k \delta_{pq} + \mu l_p n_q + \mu l_q n_p \,, \tag{1}$$

where p=1, 2, 3 and q=1, 2, 3 represent X, Y, Z directions, λ and μ are the Lame constants, δ_{pq} is 1 while p=q, otherwise is 0, l_q are the components of the slip vector at the fault, and n_p are the components of the normal vector to the fault.

In a homogenous and isotropic media, the wave produced by a seismic source contains three terms:

$$\mathbf{u}(\mathbf{x},t) = \mathbf{u}_{\text{near}} + \mathbf{u}_{\text{intermediate}} + \mathbf{u}_{\text{far}} \,, \tag{2}$$

where, $\mathbf{x}$ is the position vector of receivers and t is time. As indicated by eq.(2), three parts,

which are the near-field term $\mathbf{u}_{\text{near}}$, the intermediate-field term $\mathbf{u}_{\text{intermediate}}$ and the far-field term $\mathbf{u}_{\text{far}}$, are contained in the seismic wave field $\mathbf{u}(\mathbf{x}, t)$, where the three terms are distinguished by the decrease of amplitudes with distance. The near- and intermediate-field terms decrease as r^{-2} and the far-field term as r^{-1}, where r is the source-receiver distance. Consequently, there is no need to distinguish between the near- and intermediate-field terms and both terms are classified as the near-field terms in this study. In the moment-tensor inversion, the source-receiver distance is commonly quite large and the far-field term is supposed to be the predominant part in seismic waves. Because the compressional wave (P-wave) velocity is higher than the shear wave (S-wave) velocity, the P wave is commonly used to invert moment tensors independently (Ohtsu 2008). In the homogeneous and isotropic media, the P-wave amplitude excited by a point source and recorded by a receiver can be written as:

$$A_n(\mathbf{x},t) = \frac{r_n}{4\pi\rho\alpha^3 R}\cdot\begin{pmatrix} r_1 & r_2 & r_3 \end{pmatrix}\begin{bmatrix} m_{11} & m_{12} & m_{13} \\ m_{12} & m_{22} & m_{23} \\ m_{13} & m_{23} & m_{33} \end{bmatrix}\begin{bmatrix} r_1 \\ r_2 \\ r_3 \end{bmatrix}\cdot\dot{S}(t-\frac{R}{\alpha}), \quad (3)$$

where, $A_n(\mathbf{x},t)$ is the P wave, ρ is the density, α is the P-wave velocity, r_n are the direction cosine from sources to receivers, R is the source-receiver distance, m_{pq} are the moment-tensor components, and $S(t)$ is the source-time function. The far-field range may be dependent on the wave velocity, frequency, positions of receivers, number of receivers, source mechanism and source-time function, and all these factors will be analyzed in the next.

In this study, the moment tensors are inverted using the P-wave amplitudes. In addition, we use the standard moment tensor decomposition (Vavryčuk 2015), which decomposes moment tensors into isotropic (ISO), double-couple (DC) and compensated linear vector dipole (CLVD). The corresponding orthonormal form of a moment tensor can be written as:

$$\mathbf{M} = M_1\mathbf{e}_1\mathbf{e}_2 + M_2\mathbf{e}_2\mathbf{e}_2 + M_3\mathbf{e}_3\mathbf{e}_3, \quad (4)$$

where $M_1 \geq M_2 \geq M_3$ and vectors $\mathbf{e}_1$, $\mathbf{e}_2$ and $\mathbf{e}_3$ define the tensile, neutral and pressure axes, respectively. Then the moment tensor **M** can be decomposed into the three components and written as:

$$\mathbf{M} = M_{\mathrm{ISO}}\mathbf{E}_{\mathrm{ISO}} + M_{\mathrm{DC}}\mathbf{E}_{\mathrm{DC}} + M_{\mathrm{CLVD}}\mathbf{E}_{\mathrm{CLVD}}, \tag{5}$$

where $\mathbf{E}_{\mathrm{ISO}}$, $\mathbf{E}_{\mathrm{DC}}$ and $\mathbf{E}_{\mathrm{CLVD}}$ are the ISO, DC and CLVD elementary tensors. Then the relative scale factors C_{ISO}, C_{DC} and C_{CLVD} are defined as:

$$\begin{bmatrix} C_{\mathrm{ISO}} \\ C_{\mathrm{CLVD}} \\ C_{\mathrm{DC}} \end{bmatrix} = \frac{1}{M} \begin{bmatrix} M_{\mathrm{ISO}} \\ M_{\mathrm{CLVD}} \\ M_{\mathrm{DC}} \end{bmatrix}, \tag{6}$$

where $M = |M_{\mathrm{ISO}}| + |M_{\mathrm{CLVD}}| + |M_{\mathrm{DC}}|$.

2.2 Source-time function and source mechanisms

The source-time function is extremely important, because the relative magnitude of different terms is dependent on the source-time function. In many studies, the source-time function is supposed to be a Heaviside step function (Ohtsu 2008), because its derivative is the impulse function, which can simplify the inversion equation for moment tensors. However, the step function is not suitable for calculating synthetic seismic waves, because it is too idealized and different from the observations. Here, the source-time function is expressed according to Ohtsu (1995) as:

$$S(t) = \begin{cases} \dfrac{t}{T_{\mathrm{r}}} - \dfrac{2}{3\pi}\sin\left(\dfrac{2\pi t}{T_{\mathrm{r}}}\right) + \dfrac{1}{12\pi}\sin\left(\dfrac{4\pi t}{T_{\mathrm{r}}}\right) & t < T_{\mathrm{r}} \\ 1 & t \geq T_{\mathrm{r}} \end{cases}, \tag{7}$$

where T_{r} is the rise time. t is time. The source-time function in eq.(7) is broadband with its maximum at the zero Hz. The source-time function, far-field waveform and amplitude spectra of the far-field waves are plotted in Fig.1.

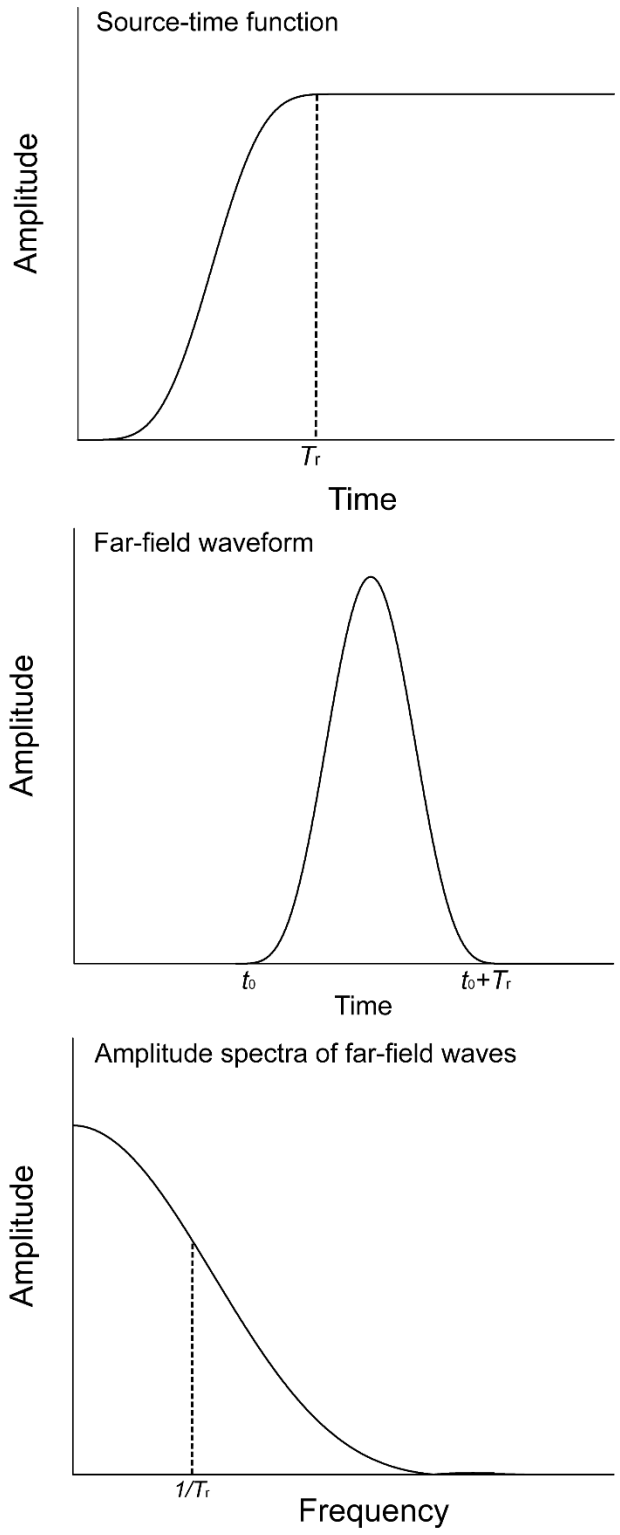

Figure 1. Source-time function, far-field waveform and amplitude spectra of the far-field waves.

The length of wave affected area is $\alpha \times T_r$. Then the predominant wavelength can be approximately equal to $\alpha \times T_r$ and the predominant frequency can be approximately equal to $1/T_r$. Actually, $1/T_r$ is also close to the central frequency of the spectrum of the far-field waves.

In the engineering practice, the source dimension and frequency of radiated waves vary greatly because the frequency depends on the size of the source area. However, if the far-field range is expressed in the number of wavelengths, the dependence on the source dimension and frequency of radiated waves is eliminated. The moment tensors for the shear dislocation, tensile dislocation and isotropic source are expressed as follows:

$$\mathbf{M}_{\text{shear}} = \begin{bmatrix} 0 & 1 & 0 \\ 1 & 0 & 0 \\ 0 & 0 & 0 \end{bmatrix} \quad \mathbf{M}_{\text{tensile}} = \begin{bmatrix} 1 & 0 & 0 \\ 0 & \dfrac{\lambda}{\lambda+2\mu} & 0 \\ 0 & 0 & \dfrac{\lambda}{\lambda+2\mu} \end{bmatrix} \quad \mathbf{M}_{\text{isotropic}} = \begin{bmatrix} 1 & 0 & 0 \\ 0 & 1 & 0 \\ 0 & 0 & 1 \end{bmatrix}, \tag{8}$$

where λ and μ are the Lame constants.

2.3 Positions of receivers

In general, six one-component receivers are needed to invert for a moment tensor. In this study, the positions of receivers are defined as:

$$\mathbf{r}_{\text{rec}}^{n} = R\mathbf{e}_{\text{azi}} + R_{\text{r}}\mathbf{e}_{\text{rel}}^{n}, \tag{9}$$

where $\mathbf{r}_{\text{rec}}^{n}$ is the direction vector pointing from the source to the nth receiver, R is the source-receiver distance, $\mathbf{e}_{\text{azi}}$ is the unit vector pointing from the source to the central point of the distribution region of receivers, R_{r} is the radius of the circle (as shown in Fig.1) and indicates the size of the distribution region of receivers, $\mathbf{e}_{\text{rel}}^{n}$ is the unit vector pointing from the center of the distribution region of receivers to the nth receiver. For simplicity, the distribution of receivers is defined as a regular-pentagonal configuration, which one receiver locates at the center of the region and the other five locate around. This configuration has been proved superior to suppress the effect of noise on the moment-tensor inversion (Kong *et al.* 2019).

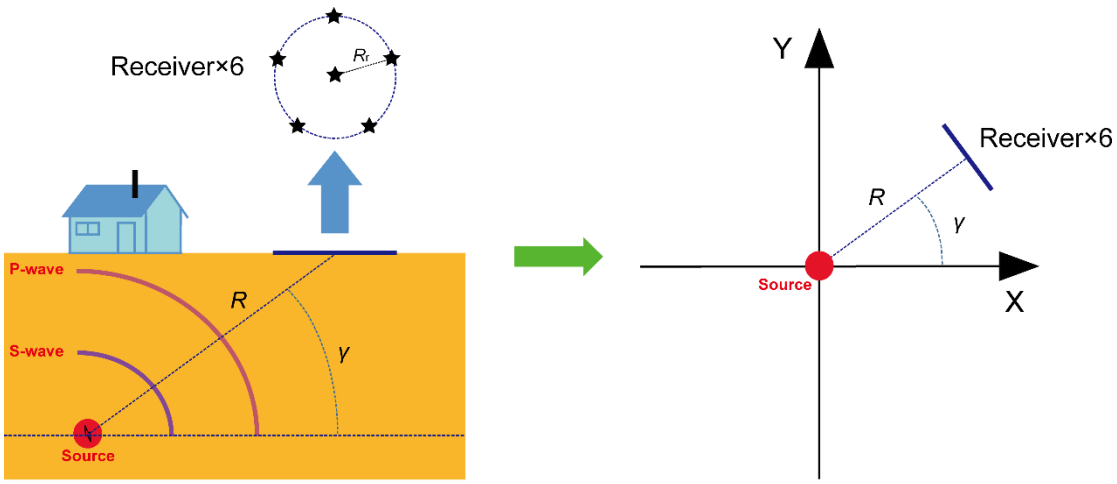

Figure 2. Positions of the six receivers, which are represented by the five-pointed stars (a). In the calculation, a setting is made that the plane with receivers is perpendicular to the line from the source to the center of the plane (b).

In Fig.2, the angle γ defines the direction of receivers and the distribution of receivers with varying azimuthal gap is investigated in the next. In real engineering applications, receivers are typically arranged as Fig.2 (a). However, when angle γ is close to 0° or 180°, the source is close to the plane with receivers and the inversion equation for moment tensors is ill conditioned. Consequently, the plane with receivers is set perpendicular to the line from the source to the center of the plane (as shown in Fig.2 (b)). Because R_r is much smaller than R, this setting has little effect on the far-field distance. For simplicity, R_r is supposed to be proportional to R and written as $R_r=\eta R$. The sensitivity of far-field range to parameter η is investigated in Section 3.3.

3 Far-field range

In this section, the far-field range is calculated and expressed in wavelengths of radiated waves. The far-field range is related to the relative magnitude of the two field terms, which vary greatly with the direction, as shown in Fig.3. The circumferential coordinate represents the direction of receivers and the radial coordinate represents the amplitude of waves.

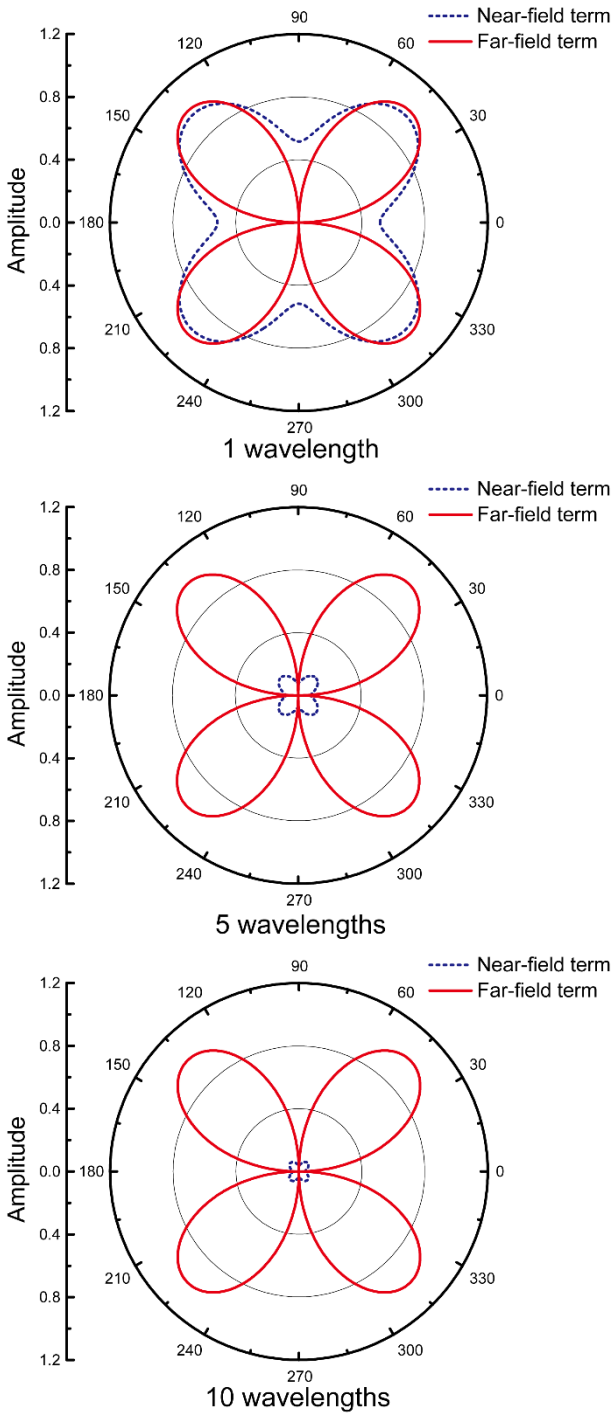

Figure 3. For the shear dislocation, the relative magnitude of the two field terms at different source-receiver distances. The circumferential coordinate represents the direction of receivers and the radial coordinate represents the amplitude of waves.

Obviously, the far-field range is dependent on the positions of receivers relative to sources. With the increase of the source-receiver distance, the effect of the near-field term on moment-tensor solutions decreases and the inversion results are more close to the true value. For the shear dislocation, the actual proportion of the DC component in the moment tensor is

100%. Because of the effect of the near-field term, the inversion results become approximate and the DC component is distorted. As shown in Fig.3, in the directions of the nodal lines of the far-field P waves, the amplitude of the far-field term is zero and the near-field term becomes significant (Vavrycuk 1992), which indicates that the corresponding far-field distance may be quite different from those in the directions far from the nodal lines. In this study, we use different displacement components in different directions to invert moment tensors. Specifically, in the directions of -45° (315°) ~45° and 135°~225°, the X displacement component is used. In the directions of 45°~135° and 225°~315°, the Y displacement component is used. Thus, in the inversion, the amplitude of the corresponding displacement component of the far-field term is relatively large and has a better signal-to-noise ratio.

The change of the proportion of the DC component in the moment tensors is plotted in Fig.4. Several directions, which are γ=15°, 25°, 35°and 45°, are considered in Fig.4. The source-receiver distance in the horizontal axis is expressed in wavelengths of radiated waves.

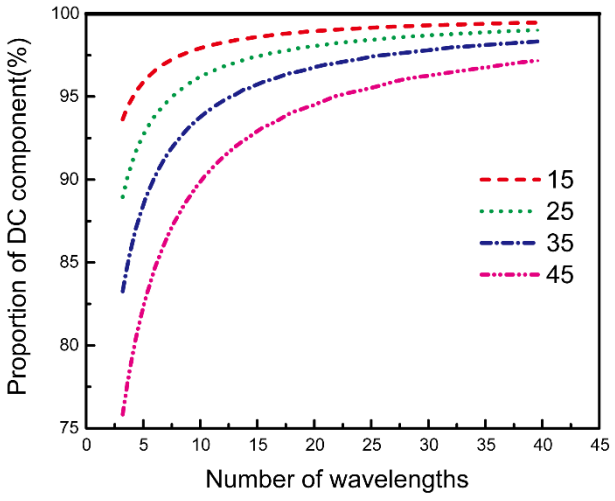

Figure 4. For the shear dislocation, the change of the proportion of the DC component in moment tensors with the increase of source-receiver distance in different directions, γ=15°, 25°, 35°and 45°.

Fig.4 suggests that the effect of the near-field term on the retrieved DC component changes with directions and is extremely difficult to be eliminated. For the purpose of this

study, we define the far-field range as a source-receiver distance, beyond which the error of the proportion of the DC component is less than 5%, and call as the far-field distance. In the next sections, the far-field distance is calculated and its sensitivity to the wave velocity, frequency, receivers and source mechanism is analyzed.

3.1 Wave velocity

According to Schön (2016), the wave velocity in common rock is among the range of 2000-9000m/s. The far-field distance is plotted in Fig.5, in which the wave velocity is plotted on the X axis, the direction of receivers γ is plotted on the Y axis and the corresponding far-field distance expressed in wavelengths is given by the Z axis. The projection of the surface in the directions of γ=10°, 15°, 20°, 25°, 30°, 35°, 40°, 45° is plotted on the X-Z plane. The color bar represents the number of wavelengths. The directions above are representative, because the radiation patterns of the two field terms are all symmetrical (as shown in Fig.3).

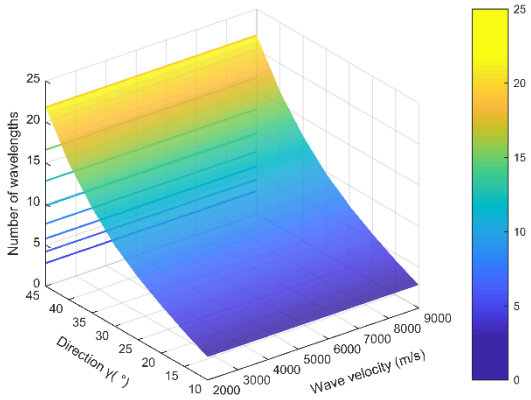

Figure 5. Far-field distances for different wave velocities in different directions.

As shown in Fig.5, the far-field distance is not affected by the wave velocity, even though the velocity is present in the formula for the Green's function. Because the far-field distance is independent of the velocity, the definition of far-field range obtained in the homogeneous and isotropic media can be applied to the moment-tensor inversion in a more

complex media. As long as the propagation path of seismic waves is known, the propagation distance expressed in the number of wavelengths can be calculated easily and compared with the far-field distance directly.

3.2 Wave frequency

The wave frequency used in this study indicates the predominant frequency of seismic waves. For the generality of the conclusions in this study, the wave frequency range considered in this study is 10^{-1}-10^{7}Hz, for the application of the moment-tensor inversion is not limited to earthquakes, but also to hydrofractures and acoustic emissions, in which the frequency of waves is different (Cai *et al.* 2007). The far-field distances for different frequencies are plotted in Fig.6, in which the wave frequency is plotted on the X axis, the direction of receivers γ is plotted on the Y axis and the corresponding far-field distance expressed in wavelengths is given by the Z axis. The projection of the surface in the directions of γ=10°, 15°, 20°, 25°, 30°, 35°, 40°, 45° is plotted on the X-Z plane.

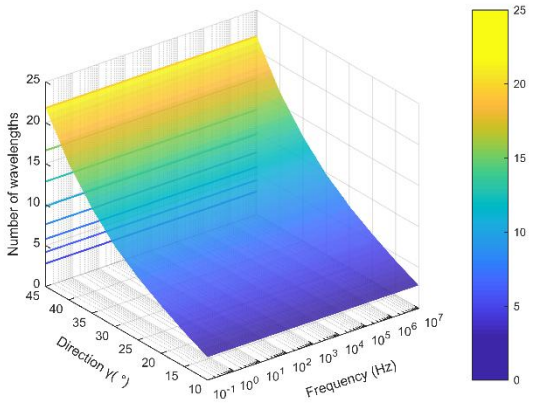

Figure 6. Far-field distances for different wave frequencies in different directions.

Fig.6 suggests that the far-field distance is independent of the wave frequency, which indicates that the conclusions obtained in this study is suitable for the moment-tensor inversion in various applications.

3.3 Receivers

In the traditional guideline for the moment-tensor inversion, it is desirable that the number of receivers should be as many as possible and the distribution region of receivers should be as large as possible to cover the focal sphere adequately (Eyre & Der Baan 2015). Consequently, in this section, we study the far-field distance with different distances between receivers and numbers of receivers.

The radius of the circle R_r, which represents the distance between receivers, is supposed to be proportional to the source-receiver distance R (written as $R_r=\eta R$) and the ratio η is set to be 0.1, 0.2, 0.3, 0.4 ,0.5. The far-field distances for different ratios in different directions are plotted in Fig.7. In Fig.7, the directions near the nodal lines are excluded from the moment-tensor inversion, because the far-field distances in these directions are heavily dependent on the displacement component used in the inversion and need to be discussed separately.

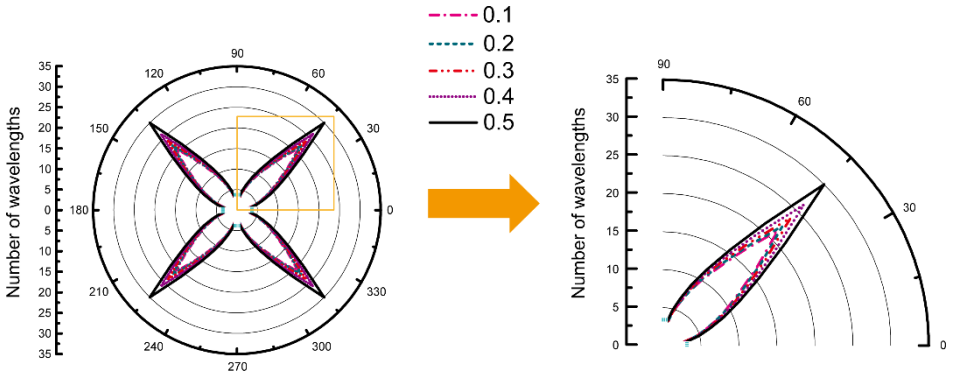

Figure 7. Far-field distances for different ratios in different directions. The directions close to the nodal lines are excluded from the moment-tensor inversion and represented by the light-colored symbols.

According to Fig.7, if only the directions far from the nodal lines are considered, the maximum far-field distance is along the directions of 45°, 225°, 135° and 315°, which are the tensile and pressure axes of the source, respectively. As the parameter η increases, the far-field distance increases, which indicates that large distribution region of receivers is

harmful to the accuracy of moment-tensor solutions. This conclusion contradicts to the formal guideline of the distribution of receivers provided the Green's functions are calculated using the far-field approximation. The reason is that the proportions of the near-field term in the signals obtained by different receivers are different. According to Fig.3, as the distance between receivers increases, the difference of the proportions of the near-field term in the signals obtained by different receivers increases. The principle of the moment-tensor inversion is to identify the radiation pattern of the seismic waves through the receivers, and then identify the corresponding dislocation type of the source. The difference of the proportions can distort the radiation pattern of the far-field term and its increase will lead to great errors.

In the directions (-10°~10°, 80°~100°, 170°~190° and 260°~280°) close to the nodal lines of the far-field P waves, the far-field distances are heavily dependent on the displacement component used to invert moment tensors. The radiation patterns plotted by the displacement components are shown in Fig.8.

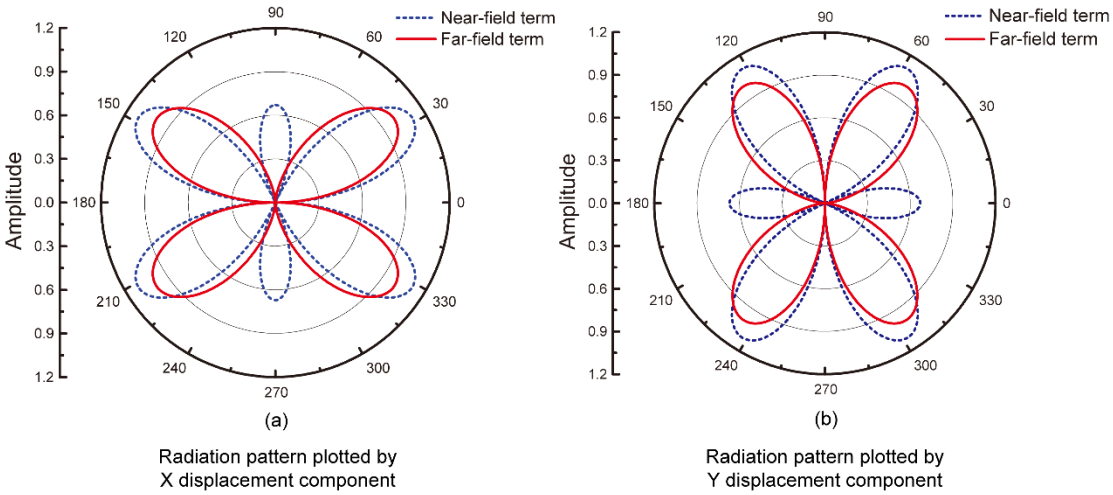

Figure 8. For the shear dislocation, the relative magnitude of the displacement components of the two field terms at the source-receiver distance of 1 wavelength. The circumferential coordinate represents the direction of receivers and the radial coordinate represents the amplitude of the displacement

component.

In the directions near 0° and 180° (corresponding to the X axis in the Cartesian coordinate system), the far-field distances calculated by the X displacement component is quite small, because the X displacement component of the near-field term is close to zero (as shown in Fig.8 (a)). However, if we use the Y displacement component to invert moment tensors, we can not determine the far-field distance, because the Y displacement component of the far-field term is zero and that of the near-field term is relatively large (as shown in Fig.8 (b)). In the directions near 90° and 270° (corresponding to the Y axis in the Cartesian coordinate system), things are the same, except that we should use the Y displacement component to invert moment tensors. In the directions far from the nodal lines, the difference of the far-field distances caused by different displacement components is quite small, because both the X and Y displacement components of the near-field term are relatively large. More generally, in the directions close to the nodal lines, the displacement component used in the inversion should be as parallel as possible to the wave propagation direction. Otherwise, great errors of moment-tensor solutions can be observed.

Fig.8 also indicates that in the directions near the tensile and pressure axes (45°, 135°, 225° and 315°), the magnitude of the near-field term relative to the far-field term is very large and the change of the near-field term is very dramatic. The combination of these two causes seriously distorts the radiation pattern of the far-field term and results in long far-field distances.

In addition, increasing the number of receivers can suppress the effect of the near-field term on moment-tensor solutions. We use 10 receivers to invert moment tensors and the far-field distances are plotted in Fig.9. The configuration with 10 receivers is that 4 receivers

locate near the center and the others locate around at equal intervals, which is similar to the configuration with 6 receivers in Fig.2 and can achieve a relatively small condition number for the inversion equation.

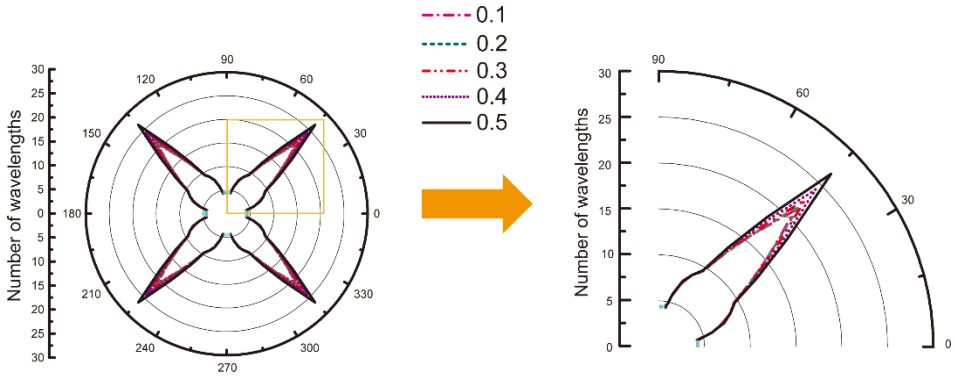

Figure 9. For the configuration with 10 receivers, the far-field distances for different ratios in different directions.

In Fig.9, the directions near the nodal lines are also excluded from the moment-tensor inversion. If the number of receivers changes from 6 to 10, the maximum far-field distance changes from 30 to 26.6 wavelengths, which indicates that the usage of more receivers is helpful for the accuracy of moment-tensor solutions. In addition, the shape of the curve near the nodal lines in Fig.9 is slightly different from that in Fig.7. In the calculations of Fig.7 and Fig.9, we use the X or Y displacement component instead of the radial component of displacement. In different configurations of receivers, the relative positions of receivers to the source are slightly different. This difference has minor effect on the far-field distance in the directions near the nodal lines.

3.4 Tensile dislocation and isotropic source (explosion or implosion)

The conclusions above are for the shear dislocation, because the shear dislocation is of great interest in seismology. Actually, tensile dislocations and isotropic sources are also quite common in some engineering applications. For the consistency of the study, we are still concerned about the DC component in the moment tensors of tensile dislocations and

isotropic sources.

For the pure tensile dislocation, the actual proportion of the DC component is 0. In moment-tensor solutions, the change of the proportion of the DC component with the increase of source-receiver distance is plotted in Fig.10.

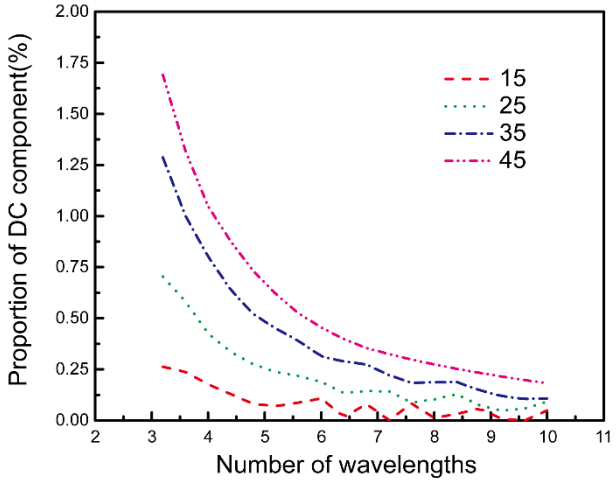

Figure 10. For the tensile dislocation, the change of the proportion of the DC component in moment tensors with the increase of source-receiver distance in different directions, γ=15°, 25°, 35°and 45°.

By comparing Fig.10 with Fig.4, the effect of the near-field term on the moment-tensor inversion for tensile dislocations is much smaller than that for shear dislocations, thus the far-field distance is much shorter for the tensile dislocation. According to the radiation patterns of the two terms of the tensile dislocation (as shown in Fig.11), the amplitude of the near-field term decreases more quickly than that of the shear dislocation. In addition, the radiation pattern of the near-field term is similar to that of the far-field term, which can reduce the effect of the near-field term on moment-tensor solutions.

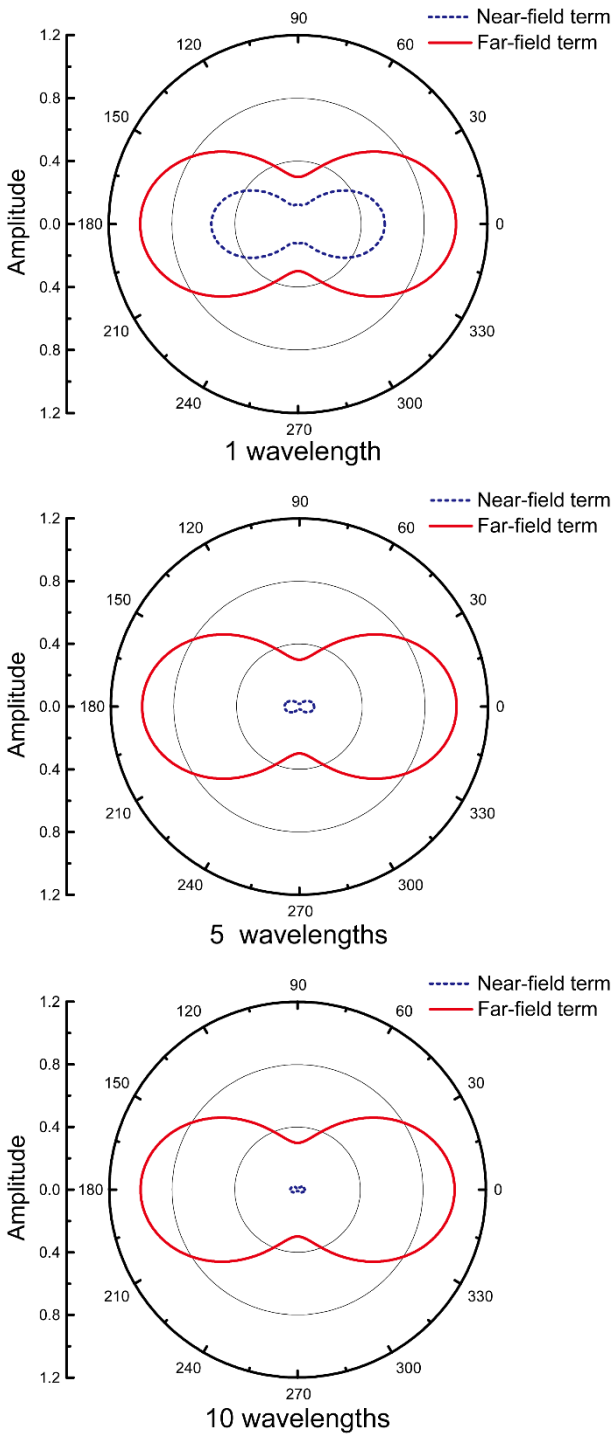

Figure 11. For the tensile dislocation, the relative magnitude of the two field terms at different source-receiver distances

For the isotropic source (explosion or implosion), there is no effect of the near-field term on the moment-tensor inversion, because the radiation pattern of the far-field term is exactly the same as that of the near-field term (as shown in Fig.12). It should be noted that the two curves have been normalized by the maximum value respectively in order to compare the

shapes of the two curves. Actually, the value of the far-field term is much larger than that of the near-field term.

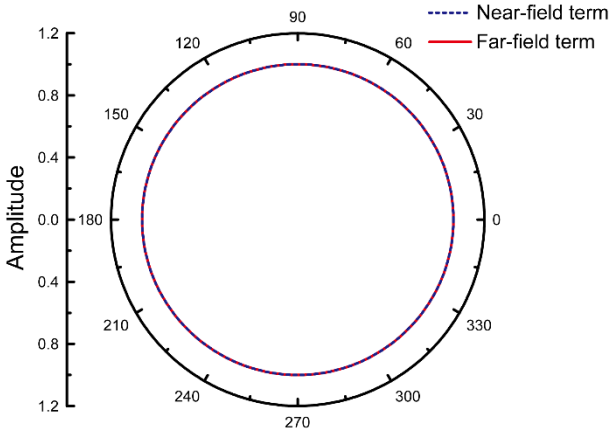

Figure 12. Radiation patterns of the near- and far-field terms.

Based on the results above, it can be concluded that the far-field distance for the shear dislocation is higher than for other dislocation types. Consequently, for all moment-tensor inversions, keeping the source-receiver distance larger than the maximum value of the far-field distance for the shear dislocation is recommended for achieving a sufficient accuracy.

4 Conclusion

In the moment-tensor inversion, clarifying far-field range is extremely important for improving the accuracy of source mechanisms, when the far-field Green's function are applied. In this study, the explicit far-field range is determined based on the errors of moment-tensor solutions, and the sensitivity of far-field range to several factors is analyzed. Based on the numerical experiments, we arrived at the following conclusions:

1. The far-field distance, which is expressed as the number of wavelengths of radiated waves, is not related to the wave velocity, thus the conclusions obtained in the homogeneous and isotropic media can be applied to more complex media, such as the layered media. In the layered media, the ratio of the propagation distance to the wavelength can be calculated in

each layer along the wave propagation path and the sum of the ratios can be compared with the far-field distance directly.

2. The far-field distance is not related to the wave frequency, thus the explicit definition of far field in this study can be applied to many other applications, such as hydraulic fracturing and acoustic emissions with a broad range of radiated frequencies.

3. If the far-field assumption is applied, a near-source position of receivers is harmful to the accuracy of moment-tensor solutions. The common recommendation is to use a large coverage of receivers but of course with the Green's function calculated accurately, i.e. including the near-field waves.

4. The far-field distance differs in different directions. For the shear dislocation, in the directions near the nodal lines of the far-field P waves, the far-field distances are heavily dependent on the displacement component used to invert moment tensors. The radial component of displacement, which is parallel to the wave propagation direction, is recommended for the inversion and the corresponding far-field distance is quite short. Otherwise great errors of the moment-tensor solutions will be caused and the far-field distances can not be determined. In the directions far from the nodal lines, the difference of the far-field distances calculated by different displacement components is very small. The maximum far-field distance appears in the directions of the pressure and tensile axes of the source and the value is about 30 wavelengths.

5. Using more receivers (>6) in the moment-tensor inversion can suppress the effect of the near-field term on the solutions and shorten the far-field distance.

6. For the tensile dislocation and isotropic source (explosion or implosion), the effect of

the near-field term on moment-tensor solutions is small and can be ignored in the moment-tensor inversion.

ACKNOWLEDGMENTS

The authors of this paper would like to thank the financial supports provided by the Strategic Priority Research Program of Chinese Academy Sciences (Grant No. XDA22000000).

REFERENCES

Aki, K. & Patton, H., 1978. Determination of seismic moment tensor using surface waves, *Tectonophysics,* 49**,** 213-222.

Aki, K. & Richards, P.G., 2002. *Quantitative seismology*, University Science Books, Sausalito, CA.

Cai, M., Kaiser, P.K., Morioka, H., Minami, M., Maejima, T., Tasaka, Y. & Kurose, H., 2007. FLAC/PFC coupled numerical simulation of AE in large-scale underground excavations, *International Journal of Rock Mechanics and Mining Sciences,* 44**,** 550-564.

Cesca, S., Buforn, E. & Dahm, T., 2006. Amplitude spectra moment tensor inversion of shallow earthquakes in Spain, *Geophysical Journal International,* 166**,** 839-854.

Der Baan, M.V., Eaton, D.W. & Preisig, G., 2016. Stick-split mechanism for anthropogenic fluid-induced tensile rock failure, *Geology,* 44**,** 503-506.

Dziewonski, A.M., Chou, T.A. & Woodhouse, J.H., 1981. Determination of earthquake source parameters from waveform data for studies of global and regional seismicity, *Journal of Geophysical Research,* 86**,** 2825-2852.

Eaton, D.W., van der Baan, M., Birkelo, B. & Tary, J.-B., 2014. Scaling relations and spectral characteristics of tensile microseisms: evidence for opening/closing cracks during hydraulic fracturing, *Geophysical Journal International,* 196**,** 1844-1857.

Eyre, T.S. & Der Baan, M.V., 2015. Overview of moment-tensor inversion of microseismic events, *The Leading Edge,* 34**,** 882-888.

Fojtíková, L., Vavryčuk, V., Cipciar, A. & Madarás, J., 2010. Focal mechanisms of micro-earthquakes in the Dobrá Voda seismoactive area in the Malé Karpaty Mts.(Little Carpathians), Slovakia, *Tectonophysics,* 492**,** 213-229.

Graham, C.C., Stanchits, S., Main, I.G. & Dresen, G., 2010. Comparison of polarity and moment tensor inversion methods for source analysis of acoustic emission data, *International Journal of Rock Mechanics and Mining Sciences,* 47**,** 161-169.

Hardebeck, J.L. & Shearer, P.M., 2003. Using S/P Amplitude Ratios to Constrain the Focal Mechanisms of Small Earthquakes, *Bulletin of the Seismological Society of America,* 93**,** 2434-2444.

Hudson, J.A., Pearce, R.G. & Rogers, R.M., 1989. Source type plot for inversion of the moment tensor, *Journal of Geophysical Research,* 94**,** 765-774.

Jechumtalova, Z. & Silený, J., 2005. Amplitude ratios for complete moment tensor retrieval,

Geophysical Research Letters, 32.

Kanamori, H. & Given, J.W., 1981. Use of long-period surface waves for rapid determination of earthquake-source parameters, *Physics of the Earth and Planetary interiors,* 27**,** 8-31.

Kanamori, H. & Given, J.W., 1982. Use of long-period surface waves for rapid determination of earthquake source parameters 2. Preliminary determination of source mechanisms of large earthquakes (MS⩾ 6.5) in 1980, *Physics of the Earth and Planetary Interiors,* 30**,** 260-268.

Kong, Y., Li, M. & Chen, W.M., 2019. Sensor arrangement in moment-tensor inversion for cracks, *Journal of Beijing University of Aeronautics and Astronautics,* 45, 1380-1387 (in Chinese).

Legrand, D., Kaneshima, S. & Kawakatsu, H., 2000. Moment tensor analysis of near-field broadband waveforms observed at Aso Volcano, Japan, *Journal of Volcanology and Geothermal Research,* 101**,** 155-169.

Liu, P.X., Chen, S.Y., Guo, Y.S. & Li, P.C., 2014. Moment tensor inversion of acoustic emission, *Chinese J. Geophys,* 858-866 (in Chinese).

Lizurek, G., 2017. Full Moment Tensor Inversion as a Practical Tool in Case of Discrimination of Tectonic and Anthropogenic Seismicity in Poland, *Pure Appl. Geophys.,* 174**,** 197-212.

Lokmer, I. & Bean, C.J., 2010. Properties of the near-field term and its effect on polarisation analysis and source locations of long-period (LP) and very-long-period (VLP) seismic events at volcanoes, *Journal of Volcanology and Geothermal Research,* 192**,** 35-47.

Nissen-Meyer, T., Fournier, A. & Dahlen, F.A., 2007. A two-dimensional spectral-element method for computing spherical-earth seismograms - I. Moment-tensor source, *Geophysical Journal International,* 168**,** 1067-1092.

Ohtsu, M., 1988. Source inversion of acoustic emission waveform, *Doboku Gakkai Ronbunshu,* 1988**,** 71-79.

Ohtsu, M., 1995. Acoustic Emission Theory for Moment Tensor Analysis, *Research in Nondestructive Evaluation,* 6**,** 169-184.

Ohtsu, M., 2008. Moment tensor analysis. *Acoustic Emission Testing,* pp. 175-200, Springer.

Ohtsu, M. & Ono, K., 1988. AE source location and orientation determination of tensile cracks from surface observation, *NDT International,* 21**,** 143-150.

Schön, J.H., 2016. *Peysical properties of rocks,* Petroleum Industry Press, Beijing (in Chinese).

Silený, J., 2009. Resolution of non-double-couple mechanisms; simulation of hypocenter mislocation and velocity structure mismodeling, *Bulletin of the Seismological Society of America,* 99**,** 2265-2272.

Silený, J., Panza, G.F. & Campus, P., 1992. Waveform inversion for point source moment tensor retrieval with variable hypocentral depth and structural model, *Geophysical Journal International,* 109**,** 259-274.

Sipkin, S.A., 1986. Interpretation of non-double-couple earthquake mechanisms derived from moment tensor inversion, *Journal of Geophysical Research,* 91**,** 531-547.

Stierle, E., Vavrycuk, V., Kwiatek, G., Charalampidou, E.M. & Bohnhoff, M., 2016. Seismic moment tensors of acoustic emissions recorded during laboratory rock deformation experiments: sensitivity to attenuation and anisotropy, *Geophysical Journal International,* 205**,** 38-50.

Tape, W. & Tape, C., 2012. A geometric comparison of source-type plots for moment tensors, *Geophysical Journal International,* 190**,** 499-510.

Toyokuni, G. & Takenaka, H., 2006. FDM computation of seismic wavefield for an axisymmetric earth with a moment tensor point source, *Earth Planets Space,* 58**,** E29-E32.

Trifu, C.I., 2000. A Fast Evaluation of the Seismic Moment Tensor for Induced Seismicity, *Bulletin of*

the Seismological Society of America, 90**,** 1521-1527.

Van Driel, M. & Nissenmeyer, T., 2014. Seismic wave propagation in fully anisotropic axisymmetric media, *Geophysical Journal International,* 199**,** 880-893.

Van Driel, M., Wassermann, J., Pelties, C., Schiemenz, A. & Igel, H., 2015. Tilt effects on moment tensor inversion in the near field of active volcanoes, *Geophysical Journal International,* 202**,** 1711-1721.

Vavrycuk, V., 1992. Polarization properties of near-field waves in homogeneous isotropic and anisotropic media: numerical modelling, *Geophysical Journal International,* 110**,** 180-190.

Vavryčuk, V., 2001. Inversion for parameters of tensile earthquakes, *Journal of Geophysical Research: Solid Earth,* 106**,** 16339-16355.

Vavryčuk, V., 2015. Moment tensor decompositions revisited, *Journal of Seismology,* 19**,** 231-252.

Vavryčuk, V., Bohnhoff, M., Jechumtálová, Z., Kolář, P. & Šílený, J., 2008. Non-double-couple mechanisms of microearthquakes induced during the 2000 injection experiment at the KTB site, Germany: A result of tensile faulting or anisotropy of a rock?, *Tectonophysics,* 456**,** 74-93.

Vidale, J.E., Goes, S. & Richards, P.G., 1995. Near-field deformation seen on distant broadband seismograms, *Geophysical Research Letters,* 22**,** 1-4.

Xu, S.D., Li, Y.H. & Liu, J.P., 2017. Detection of cracking and damage mechanisms in brittle granites by moment tensor analysis of acoustic emission signals, *Acoust. Phys.,* 63**,** 359-367.

Yu, H.Z., Zhu, Q.Y., Yin, X.C. & Wang, Y.C., 2005. Moment tensor analysis of the acoustic emission source in the rock damage process, *Progress in Natural Science,* 15**,** 609-613.